Nanoscale

PAPER

View Article Online
View Journal | View Issue

Cite this: *Nanoscale*, 2014, **6**, 996

Self-assembly of gold nanorods into vertically aligned, rectangular microplates with a supercrystalline structure†

Junyan Xiao, Zhe Li, Xiaozhou Ye, Yurong Ma and Limin Qi*

Received 8th October 2013
Accepted 2nd November 2013

DOI: 10.1039/c3nr05343a

www.rsc.org/nanoscale

Vertically aligned, supercrystalline microplates with a well-defined rectangular shape were fabricated in a large area through self-assembly of gold nanorods by a novel bulk solution evaporation method. This evaporative self-assembly strategy involving continuous movement of the contact line can prevent the coffee-ring effect, thus allowing uniform deposition of discrete GNR superstructures over a large area and favoring the formation of GNR supercrystals with geometrically symmetric shapes. A mechanism based on the continuing nucleation and growth of smectic GNR superstructures accompanying the movement of the contact line was put forward for the formation of the unique GNR supercrystal arrays. Based on this mechanism, a micropatterned substrate was designed to control the nucleation location and growth direction, leading to the spontaneous self-assembly of nearly parallel arrays of vertically aligned, supercrystalline microplates of GNRs. The obtained rectangular-plate-shaped GNR supercrystals exhibited interesting anisotropic optical reflection properties, which were revealed by polarized light microscopy.

Introduction

The self-assembly of colloidal nanocrystals into ordered superstructures has emerged as a powerful strategy for the bottom-up fabrication of nanocrystal ensembles with desirable architectures, fascinating collective properties, and promising applications in functional devices.[1–6] While a wide variety of nanoparticle superlattices assembled by spherical nanocrystals have been reported, there has been increasing interest in the fabrication of mesoscopic and macroscopic supercrystals constructed from non-spherical nanocrystals since anisotropic nanocrystals can form more abundant and complex superlattices and may offer unique characteristics due to their anisotropic nature.[7–11] Recently, the self-assembly of noble metal nanocrystals into complex plasmonic nanostructures has attracted significant attention because of their collective optical properties and potential applications as plasmonic metamaterials for sensing and nanophotonics.[11–16] Thanks to the remarkable advance in controlled synthesis of gold nanorods (GNRs) with unique plasmonic properties,[17–19] considerable progress has been made in the spontaneous self-assembly of GNRs into 2D and 3D superstructures with long-range ordering of supercrystals.[20–28] However, it remains a challenge to develop facile and controllable self-assembly approaches toward discrete GNR supercrystals with well-defined morphologies and to achieve hierarchical arrangement of supercrystalline building blocks.

Controlled evaporative self-assembly has been widely regarded as a very simple yet robust method to assemble diverse nanoparticles into complex ordered superstructures.[29] A well-known example is the deposition of "coffee rings" when colloidal particles are carried to the pinned contact line of drying droplets by outward flowing of solvents towards the edge. Wang *et al.* first demonstrated the formation of large-area, 3D ordered GNR superstructures by droplet evaporation.[20] Smectic and nematic phase superstructures of GNRs capped by cetyltrimethylammonium bromide (CTAB) can be obtained in the circular ring area of the dried droplet. Adopting a similar droplet evaporation method, Liz-Marzán *et al.* successfully fabricated standing superlattices of GNRs capped by a cationic gemini surfactant in the ring area.[21] Later on, the self-assembly of island-like, highly organized GNR supercrystals was achieved by slow droplet evaporation in a humid atmosphere.[15] Despite the notable success of the drop casting evaporation in the self-assembly of GNR supercrystals, this method generally suffers from the limited area and solution volume for self-assembly and the lack of accurate control over the size, shape, and alignment of GNR supercrystals. It is noteworthy that evaporative self-assembly combined with lithographically patterned substrates can be used to realize precise placement and oriented assembly of GNRs.[30–32] Recently, Bach *et al.* reported a novel evaporation-induced self-assembly of discrete arrays of standing GNRs with

Beijing National Laboratory for Molecular Sciences, State Key Laboratory for Structural Chemistry of Unstable and Stable Species, College of Chemistry, Peking University, Beijing 100871, China. E-mail: liminqi@pku.edu.cn

† Electronic supplementary information (ESI) available. See DOI: 10.1039/c3nr05343a

precise placement on a micropatterned substrate.[28] Nevertheless, the potential of template-assisted evaporative self-assembly in controlling the shape and arrangement of GNR supercrystals is still far from fully exploited.

Herein we describe a novel evaporative self-assembly method based on bulk solution evaporation for assembling GNRs into vertically aligned, rectangular microplates with a supercrystalline structure in a large area. To the best of our knowledge, this is the first observation of vertically aligned arrays of plate-shaped supercrystals assembled from inorganic nanorods. Furthermore, nearly parallel arrays of vertical supercrystalline microplates are obtained with the assistance of a topographically patterned substrate.

Experimental section

Materials

Cetyltrimethylammonium bromide (CTAB, 98%) was purchased from Sinopharm Chemical Reagent Beijing Co. Ltd. Hydrochloroauric acid trihydrate ($HAuCl_4 \cdot 3H_2O$, 99.9%) was obtained from Beijing Chemical Reagents Co. All the other chemicals were of analytical grade and were used without further purification. The water used was deionized.

The raised stripe-patterned silicon substrates were custom made through conventional photolithography by the State Key Laboratory for Micro/Nanometer Processing Technology of China.

Synthesis of gold nanorods

CTAB-capped gold nanorods (GNRs) were synthesized by a seed-mediated method following the reported procedure[20] with minor modification. In a typical synthesis, CTAB-stabilized seeds were first synthesized by adding an aqueous $HAuCl_4$ solution (0.125 mL, 10 mM) into an aqueous CTAB solution (3.75 mL, 0.1 M) in a glass vessel. Then, a freshly prepared ice-cold aqueous $NaBH_4$ solution (0.3 mL, 10 mM) was injected quickly into the mixture solution under rapid stirring, which was kept for 2 min. The resulting seed solution was kept at 27 °C and used within 2–5 h after preparation. The growth solution of GNRs was prepared by adding aqueous solutions of $HAuCl_4$ (1.075 mL, 10 mM) and $AgNO_3$ (0.24 mL, 10 mM) into an aqueous CTAB solution (25 mL, 0.1 M) in a beaker flask. Then a freshly prepared ascorbic acid solution (0.17 mL, 0.1 M) was added and the resulting growth solution became colorless after gentle vibration. Finally, the growth of GNRs was started by adding 0.115 mL CTAB-stabilized seed solution into the growth solution. The reaction mixture was left undisturbed in a water bath kept at 27 °C for at least 5 hours, resulting in the formation of an aqueous dispersion of CTAB-capped GNRs with a GNR particle concentration of approximately 0.8 nM and a CTAB concentration of 0.1 M, where the concentration of the GNRs was determined by the Beer–Lambert law with a molar extinction coefficient of $\varepsilon = 4.6 \times 10^9\ M^{-1}\ cm^{-1}$.[33]

Self-assembly of GNR supercrystals

The as-prepared aqueous dispersion of CTAB-capped GNRs was centrifugated and redispersed in CTAB solutions repeatedly, giving concentrated GNR dispersions with varied GNR concentrations and a CTAB concentration of 1 mM. For a typical self-assembly of GNRs by bulk solution evaporation, a clean silicon square plate (~4 mm × 4 mm) with a thickness of ~0.5 mm was flatly placed at the bottom of one vessel (~6.5 mm in inner diameter) of a plastic 96-well tissue culture plate, and then 0.2 mL of GNR dispersion with a certain concentration (typically, 8 nM) was injected into the vessel with the Si plate immersed. The vessel was covered by a filter paper to slow down the solvent evaporation under ambient conditions. It normally took about 3 days to complete the evaporation. For the self-assembly of parallel arrays of plate-shaped GNR supercrystals, a raised stripe-patterned Si plate was employed to replace the pristine Si plate and the assembly was carried out under otherwise identical conditions.

Characterization

The GNRs were characterized by UV-vis absorption (Perkin-Elmer Lambda 950) and transmission electron microscopy (TEM, JEOL JEM2100, 200 kV). The GNR assemblies on the Si substrate were characterized directly by scanning electron microscopy (SEM, Hitachi FE-S4800, 10 kV) and X-ray diffraction (XRD, Rigaku DMAX-2400, Cu Kα radiation) without any post-treatment. After suitable washing with ethanol, the GNR assemblies on the Si substrate were characterized by an optical microscope (Olympus BX51TRF with DP72-SET digital camera) equipped with polarizers in reflection mode under white-light illumination.

Results and discussion

The building blocks employed for the assembly experiments were CTAB-capped GNRs synthesized using the seed-mediated method.[19,20] They were [001]-oriented single crystals with a length of 37 ± 4 nm, a diameter of 11 ± 1 nm, and an aspect ratio of ~3.4 (Fig. S1, ESI†). A small amount of gold nanoparticles (<5%) coexisted with the GNRs but they did not show considerable effect on the self-assembly of GNRs under the current assembly conditions. The self-assembly process of GNRs by bulk solution evaporation is schematically illustrated in Fig. 1a.

A clean silicon square plate ~0.5 mm in thickness was flatly placed at the bottom of a plastic vessel ~6.5 mm in inner diameter, and then 0.2 mL of aqueous dispersion of CTAB-capped GNRs (typically ~8 nM in GNR concentration with a CTAB concentration of 1 mM) was injected into the vessel with the Si plate immersed. Slow evaporation of the bulk solution resulted in a gradual decline of the solution surface with a concave meniscus (Fig. 1b), accompanied by concentration of the GNR dispersion. When the concave meniscus of the solution touched the central part of the substrate, the surface of the central part was exposed to air and a solid–liquid–gas three-phase contact line appeared (Fig. S2, ESI†). Then, the contact line receded continuously from the interior towards the substrate edge, which was accompanied by the deposition of liquid-crystalline phases of GNR superstructures on the drying

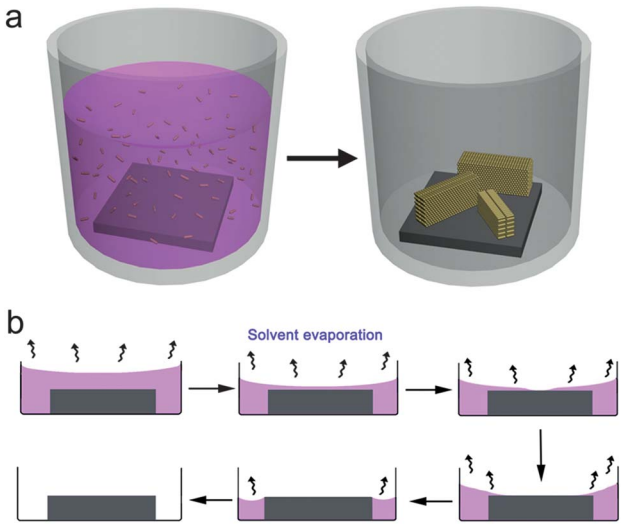

Fig. 1 (a) Schematic illustration of the experimental setup for self-assembly of GNRs *via* bulk solution evaporation. (b) Schematic side view of continuous decline of the solution surface with a concave meniscus upon solvent evaporation.

substrate. After the solvent covering the substrate was completely evaporated, plenty of GNR supercrystals with regular shapes were left on the substrate. It is worth noting that the formation of coffee rings was prevented during the bulk solution evaporation process because of the continuous movement of the contact line, leading to fairly uniform distribution of discrete GNR supercrystals over the whole surface of the Si plate.

Fig. 2a shows a representative low-magnification SEM image of the GNR superstructures formed on the substrate, suggesting the formation of ribbon-like structures with an average length of 5.4 μm over a large area. Surprisingly, these "ribbons" are actually vertically aligned, rectangular microplates, most of which are slightly inclined with respect to the direction perpendicular to the substrate (Fig. 2b). Fig. 2c shows a high-magnification SEM image of the narrow top face of a nearly upstanding microplate, which shows that the flatly aligned nanorods assemble together in a side-by-side fashion to form layers and the layers pack parallel to each other into a smectic phase superstructure. A close observation of the wide side face of a considerably tilted microplate (Fig. 2d) shows hexagonally close-packed GNRs, confirming the formation of rectangular-plate-shaped GNR supercrystals with a smectic phase. It may be noted that a few gold nanoparticles occasionally deposited on the surface of the microplates, but generally they were not incorporated inside the supercrystalline microplates owing to the self-separation of GNRs.[20] Detailed SEM observations of the rectangular microplates suggest that each supercrystalline plate generally consists of 2–7 layers of densely packed GNR arrays, resulting in a thickness around 70–260 nm (Fig. S3, ESI†). The average width of the rectangular microplates was estimated to be 1–2 μm according to the apparent widths of inclined microplates and the apparent lengths of GNRs constituting the microplates, which were obtained from detailed SEM observations (Fig. S4, ESI†). These results suggest that vertically aligned, supercrystalline microplates assembled from GNRs were obtained by a simple bulk solution evaporation method. These unprecedented GNR supercrystal arrays represent a novel hierarchical superstructure that may provide new opportunities for exploitation of their plasmonic properties and potential applications in integrated devices.

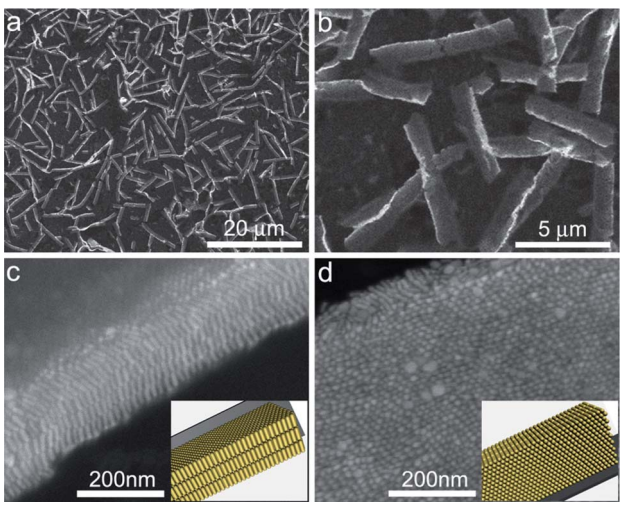

Fig. 2 (a and b) SEM images of vertically aligned, supercrystalline microplates assembled by GNRs ([GNR] = 8 nM, [CTAB] = 1 mM). (c) SEM image of an upstanding microplate showing the lying nanorods aligned in a smectic way. (d) SEM image of a tilted microplate showing the hexagonally packed, standing nanorods. Insets of (c) and (d) are the related 3D simulation models of the supercrystalline microplates viewed along different observation angles.

The concentration of the cationic surfactant CTAB in the initial GNR dispersions played a key role in the self-assembly of the vertically aligned, supercrystalline microplates by bulk solution evaporation. Our preliminary experiment showed that the self-assembly of GNRs into well-defined microplates was hard to achieve at a CTAB concentration lower than 1 mM. This result was consistent with the viewpoint that a minimum CTAB concentration (~1 mM) was required to form a bilayer on the GNR surface to stabilize them in aqueous dispersions, which was helpful for the counterbalances among the van der Waals attraction, electrostatic repulsion, interchain attraction and capillary forces.[18,20] It was found that a CTAB concentration in the range 1–2 mM was appropriate for the large-scale formation of supercrystalline microplates under the current situation. At higher CTAB concentrations, the deposition of large CTAB crystals tended to occur upon solvent evaporation, which significantly restrained the self-assembly of regular supercrystalline microplates. It is worth noting that while large dendritic CTAB crystals crystallized out of a CTAB solution (1 mM) without GNRs upon solvent evaporation, the crystallization of CTAB was considerably deteriorated in the CTAB solution (1 mM) containing GNRs. Instead of large CTAB crystals, a CTAB thin film was deposited on the substrate upon solvent evaporation, which was accompanied by the formation of standing microplates of GNRs. The CTAB thin film can be observed by manually sweeping the surface of the Si substrate

containing standing microplates; moreover, the XRD pattern of the Si substrate containing standing microplates demonstrates the presence of a lamellar structure with a *d* spacing of 2.62 nm (Fig. S5, ESI†), which is consistent with the reported laminar structure of the CTAB thin films on the Si substrate.[34,35] This CTAB thin film is an adhesive and would help fix the supercrystalline microplates standing on the substrate. Moreover, the formation of a CTAB thin film led to a positively charged substrate, which would show electrostatic repulsion towards positively charged GNRs, thus favoring the self-assembly of liquid-crystalline phases of GNRs rather than the direct attachment of individual GNRs onto the substrate.

It has been documented that for CTAB-capped GNRs, the counterbalances among the van der Waals attraction, electrostatic repulsion, interchain attraction and capillary forces would lead to the formation of liquid-crystalline phases of GNRs once the nanorod concentration is increased up to a certain point.[18] The attractive depletion force may be taken into account if the CTAB concentration in the solution is relatively high. For example, the presence of CTAB micelles (typically, the CTAB concentration is higher than 50 mM) has been shown to introduce depletion forces that enable solution-phase assembly and/or concomitant purification of Au nanocrystals.[36,37] Recently, theoretical calculation has shown that the depletion interaction is much smaller than van der Waals and electrostatic interactions during the self-assembly of CTAB-stabilized Au nanorods.[38] Therefore, the attractive depletion force due to the presence of CTAB micelles may be negligible in the current assembly process where the CTAB concentration is not high, and the interaction between CTAB-stabilized GNRs may be dominated by the van der Waals attraction, electrostatic repulsion, and interchain attraction when they approach each other. In the current situation, CTAB molecules could play an additional role, namely, forming an adhesive thin film deposited on the substrate to help fix the supercrystalline microplates standing on the substrate.

The GNR concentration in the initial GNR dispersions also plays an important role in the self-assembly of the vertically aligned, supercrystalline microplates by bulk solution evaporation. At a low GNR concentration (1.6 nM), only net-like monolayer assemblies of lying GNRs were obtained under otherwise identical self-assembly conditions (Fig. 3a). Some GNR chains formed by side-by-side assembly can be observed but a long-range ordering is lacking for the packed nanorods in the net-like assemblies (Fig. 3b). When the GNR concentration was increased to 4 nM, many discrete branch-like GNR superstructures that tended to be curly were obtained (Fig. 3c). Closer observation suggests that the branch-like assemblies consisted of several layers of GNR arrays assembled in a side-by-side mode; however, the end-to-end alignment of GNRs was considerably distorted, resulting in a considerable deviation from the smectic structure. When the GNR concentration was increased to 8 nM, a large amount of vertically aligned, supercrystalline microplates with a smectic phase can be produced, as shown in Fig. 2. These results indicate that a critical GNR concentration is required for the nucleation of the smectic phase of GNR superstructures in the solution, which would

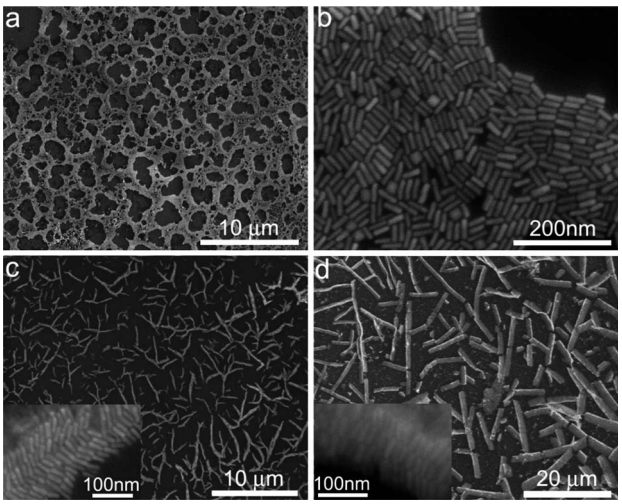

Fig. 3 SEM images of GNR assemblies obtained in aqueous GNR dispersions with different GNR concentrations: (a and b) net-like monolayer assemblies obtained at 1.6 nM ([CTAB] = 1 mM); (c) branch-like assemblies obtained at 4 nM ([CTAB] = 1 mM); (d) long-plate-like supercrystals obtained at 20 nM ([CTAB] = 2.5 mM). Insets in (c) and (d) are the enlarged SEM images showing the packing structure of GNRs.

deposit on the substrate with the receding of the contact line and further grow into well-defined microplates. If the GNR concentration was increased to 20 nM and the CTAB concentration was increased to 2.5 mM, long-plate-like supercrystals with a similar smectic structure, which had lengths up to more than 20 μm, were obtained (Fig. 3d). It may be noted that long-plate-like supercrystals can also be obtained at a CTAB concentration of 1 mM but the plates usually lie on the substrate irregularly, possibly owing to the formation of uneven CTAB thin films on the substrate in the presence of a high concentration of GNRs. The increase of the CTAB concentration from 1 mM to 2.5 mM would be favorable for keeping the long plates standing on the substrate coated by a relatively uniform thin film of CTAB.

Besides the concentrations of CTAB molecules and GNRs in the initial GNR dispersions, the temperature at which the solvent evaporates is also an important parameter that influences the formation of GNR supercrystals. At a temperature of 65 °C, the solvent evaporation was very fast, resulting in the formation of random assemblies of GNRs on the substrate (Fig. S6a and b, ESI†), which may be rationalized by considering that vigorous Brownian motion and fast solvent evaporation at this high temperature would prevent GNRs to find their favorable anchoring sites.[18] This result is reminiscent of the observation that only disordered assemblies of GNRs formed *via* droplet evaporation at a temperature higher than 60 °C.[20] When the temperature was decreased to 40 °C, dense GNR assemblies showing smectic superstructures in limited areas formed on the substrate (Fig. S6c and d, ESI†), but vertical supercrystalline microplates were not formed possibly owing to the still fast solvent evaporation. At a temperature of 25 °C, the slow solvent evaporation led to the self-assembly of GNRs into vertically aligned, rectangular microplates with a smectic superstructure,

as shown in Fig. 2. When the temperature was decreased to 15 °C, vertically aligned microplates assembled by GNRs were also obtained but there seemed to be a decrease in the regularity of the supercrystalline microplates (Fig. S6e and f, ESI†), possibly owing to a quite slower Brownian motion that was unfavorable for the GNRs to reach their stable anchoring sites. If the temperature was further decreased, large CTAB crystals tended to deposit on the substrate before the self-assembly of GNRs at the contact line, preventing the formation of supercrystalline microplates of GNRs. Therefore, an appropriate temperature is necessary for the self-assembly of GNRs into uniform supercrystalline microplates with a regular morphology.

For the self-assembly of GNRs into supercrystalline microplates by bulk solution evaporation, the gradual decrease of the solution surface with a concave meniscus as well as the consequent continuous outward movement of the contact line are indispensable, as shown in Fig. 1b. If the solvent evaporation occurred in a container with a highly hydrophobic surface, the decrease of the solution surface with a convex meniscus would result in the preferential deposition of GNR assemblies outside the Si substrate. Moreover, an appropriate contact angle of the inner surface of the container is essential for the self-assembly of uniform supercrystalline microplates. The pristine surface of the vessel used for the self-assembly of GNRs showed a contact angle around 80° toward water and the contact angle was decreased to ~38° after it was immersed in 1 mM CTAB solution for saturated adsorption of CTAB. Such a contact angle favored the formation of a concave meniscus with a suitable curvature for the self-assembly of plate-like supercrystals of GNRs. If the inner surface of the same vessel was coated by a thin layer of paraffin wax, the surface became hydrophobic with a contact angle higher than 110°, and the contact angle decreased to ~78° after it was immersed in 1 mM CTAB solution due to the adsorption of CTAB on the surface. In this case, a rather flat concave meniscus was formed and a similar assembly experiment performed in this vessel resulted in the formation of irregular assemblies of GNRs instead of regular supercrystalline microplates (Fig. S7, ESI†). Therefore, the hydrophilicity of the container is an important parameter for the self-assembly of GNR supercrystals.

For elucidation of the formation mechanism of the unique supercrystalline microplates assembled from GNRs, the GNRs in the remaining concentrated GNR dispersion beside the Si substrate were collected for TEM characterization immediately after the solution covering the Si substrate was completely evaporated, leaving a whole dried Si plate. It was observed that the GNRs were generally well dispersed while there was a tendency for the side-by-side assembly of several GNRs (Fig. S8, ESI†). This result indicates that the GNR supercrystals were not formed in solution until the assembly process occurred on the substrate, which would result from the movement of GNRs toward the continuously receding contact line. It should be pointed out that this observation cannot exclude the possibility that some nascent assemblies of GNRs formed in the solution prior to the touch of the concave meniscus to the substrate since the loose assemblies of gold nanoparticles can be easily destroyed during the process of preparation of TEM samples.[36] Nevertheless, large GNR supercrystals consisting of densely aligned GNRs, which are relatively stable, may not form before the concave meniscus of the solution touched the central part of the substrate.

Accordingly, a tentative mechanism for the self-assembly of GNRs into vertically aligned, supercrystalline microplates by bulk solution evaporation was proposed, as shown in Fig. 4. The Si substrate was first immersed in an aqueous dispersion of GNRs where an obvious concave meniscus existed at the solution surface. With the slow evaporation of solvent, the solution surface declined gradually until the lowest point of the meniscus touched the substrate to form a three-phase contact line at the central area of the substrate. Meanwhile, the progressive increase of the GNR concentration near the contact line brought about clustering of GNRs with a close-packed structure in the solution, namely, the formation of supercrystal embryos with one or a few layers of GNRs packed in a side-by-side mode. With the receding of the contact line, GNR clusters deposited on the substrate near the contact line due to the capillary forces, resulting in the nucleation of smectic GNR superstructures with GNRs lying down on the substrate. Once the nuclei consisting of several layers of hexagonally packed GNRs lying on the substrate were formed, individual GNRs and their clusters were carried to the region near the nuclei by the

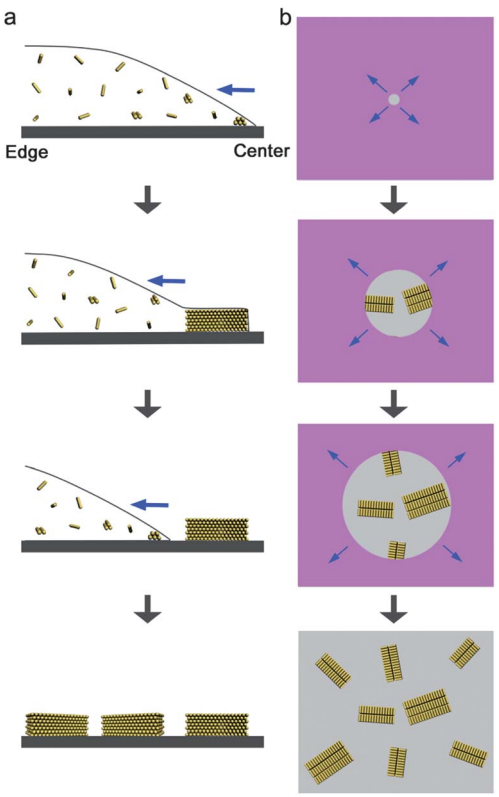

Fig. 4 Schematic illustration of the formation of vertically aligned, supercrystalline microplates *via* bulk solution evaporation with a continuously receding contact line. Side view (a) and top view (b) of the gradual movement of the contact line and the concomitant formation of plate-like supercrystals. Blue arrows refer to the direction of contact line movement.

solvent flow towards the contact line, which would tend to attach to the nuclei in a side-by-side mode. As a result, the preferential growth along the directions perpendicular to parallel GNRs led to the formation of the standing, rectangular microplates with a smectic structure. With the continuous movement of the contact line towards the edge of the substrate, individual GNRs and their clusters near the growing microplates would be depleted and the growth was stopped, which was followed by another round of nucleation and growth of supercrystalline microplates. The nucleation near the contact line and their growth into standing microplates would occur repeatedly. Finally, vertically aligned, rectangular microplates with a supercrystalline structure were left and distributed on the whole substrate after the solvent was completely evaporated. It may be pointed out that the actual assembly processes may be much more complicated than the simplified model shown in Fig. 4. For example, the contact line may not be a perfect circle and many microscale fluctuations in the contact line could exist because of unexpected perturbation, which would lead to the lack of a long-range order in the arrangement of the microplates on the substrate. Moreover, the preformed microplates on the substrate would affect the shape of the contact line and hence the assembly of the neighboring microplates, which would bring about further complexity to the assembly processes. It can be reasonably expected that improved control over the assembly processes may be achieved through deliberate design of patterned substrates and more accurate control of the condition parameters.

It is noteworthy that the bulk solution evaporation method involving continuous movement of the contact line was able to effectively avoid the deposition of coffee rings, thus allowing relatively uniform deposition of discrete GNR superstructures over the whole surface of the substrate. Moreover, the slow outwards movement of the contact line would be favorable for adequate addition of the dispersed GNRs and their clusters to the deposited crystalline nuclei, leading to the formation of GNR supercrystals with thermodynamically favored, geometrically symmetric shapes, such as regular rectangular plates.

3D GNR supercrystals have demonstrated interesting surface-enhanced Raman scattering,[15,28] two-photon-excited photoluminescence,[20] and directional optical properties[21] owing to the unique plasmonic properties of close-packed GNRs with a long-range ordering. Here we investigated the anisotropic optical reflection properties of the vertically aligned, supercrystalline microplates by polarized light microscopy. For the characterization with polarized light microscopy, the removal of the thin films of CTAB on the Si substrate is necessary as the colors arising from the film interference of the CTAB thin films would affect the observations. While washing with ethanol under drastic vibration usually led to falling down and partial destruction of the standing microplates, a large number of standing microplates can be preserved even after removal of most CTAB molecules if a gentle washing process was performed. Fig. 5 presents both normal optical micrographs and cross-polarized micrographs of the vertically aligned, supercrystalline microplates in reflection mode with different rotation angles of the sample with respect to the polarizer. It can be seen that the standing microplates did not show any noticeable difference when observed at different rotation angles using a normal light microscope. Interestingly, when observed using a cross-polarized light microscope, the microplates nearly parallel to the polarizer or analyzer direction showed negligible reflectance (dark) while the microplates oriented along the directions between the polarizer and analyzer directions showed strong reflectance (bright). Moreover, the standing microplates can switch between dark and bright when they were rotated every 45° with respect to the polarizer. In contrast, the flatly aligned microplates, which showed top surface with an isotropic hexagonally close-packed structure, did not show such switch between dark and bright with rotation (Fig. S9, ESI†). It may be noted that drastic washing with ethanol led to the partial destruction of the rectangular microplates and the GNRs disengaged from the microplates tended to form disordered assembly of GNRs on the substrate, resulting in the yellow area in the optical micrograph (Fig. S10, ESI†). These results indicated that the standing microplates exhibited remarkable

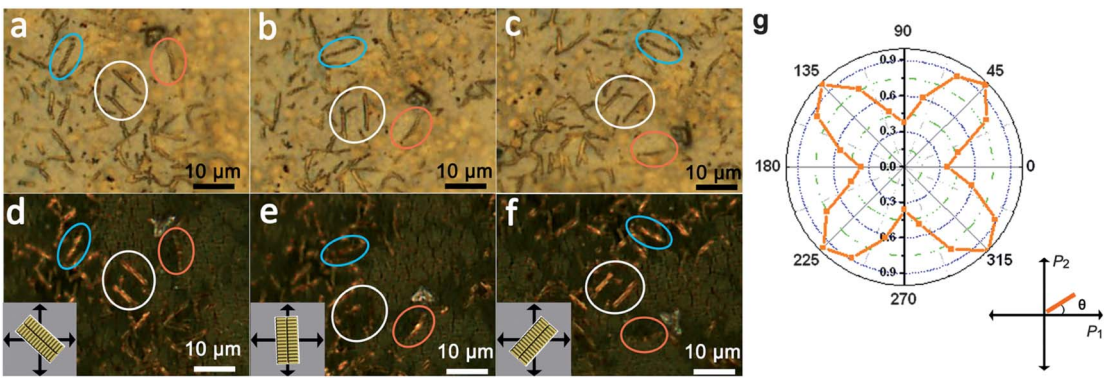

Fig. 5 Optical micrographs (a–c) and cross-polarized micrographs (d–f) of vertically aligned, supercrystalline microplates with different rotation angles: (a and d) 0°, (b and e) 45°, and (c and f) 90°. The white, blue and red circles highlight three representative areas. Insets show the orientations of a standing microplate, which represents the two parallel microplates within the white circles, relative to the directions of the polarizer (horizontal, P_1) and the analyzer (vertical, P_2). (g) Polar plot of the cross-polarized image brightness of a single vertical microplate (the longer one in the white circle) as a function of the rotary angle θ between the length direction of the microplate and the polarizer direction (P_1).

anisotropic optical properties, which provided macroscopic evidence of the long-range ordered alignment of GNRs within the plate-shaped supercrystals.

In order to give a more quantitative description of the optical reflection anisotropy of the vertical supercrystalline microplates assembled from GNRs, a polar plot of the cross-polarized image brightness of a single vertical microplate as a function of the rotary angle θ between the length direction of the microplate and the polarizer direction was measured, which is presented in Fig. 5g. It clearly shows that the image brightness maxima appear at 45°, 135°, 225°, and 315°, namely, the maximum or minimum reflectance repeats every 90°. This periodical change of the image brightness should be related to the birefringence of the vertical supercrystalline microplate consisting of GNRs aligned in a smectic state.

Considering the potential applications of micropatterned substrate-assisted assembly in controlling the location and orientation of nanorod superstructures,[28,30–32] we designed a stripe-patterned substrate to control the nucleation location and induce oriented self-assembly of GNRs into parallel supercrystalline microplates standing on trenches. The raised stripe-patterned silicon substrate was fabricated by conventional photolithography. The width and the height of the raised stripes are 3 μm and 1 μm, respectively, and their interval is 8 μm, as shown in Fig. 6a. The self-assembly of GNRs was conducted by similar bulk solution evaporation where a micropatterned silicon square plate was immersed in a GNR dispersion instead of the previously used flat Si plate. Fig. 6b shows a typical low-magnification SEM image of the left side of the substrate after GNR self-assembly, which suggests that there are a large number of nearly parallel microplates standing on the trenches between the raised stripes. An enlarged SEM image shows that these standing, rectangular microplates attached to the right walls of the trenches are nearly perpendicular (Fig. 6c).

The standing microplates had an average length of about 7 μm, slightly smaller than the width of the trenches, and the height of the standing microplates is almost identical to that of the raised stripes or walls, namely, 1 μm. It is worth mentioning that similar parallel microplates standing on the trenches were observed on the right side of the patterned Si substrate, but these microplates are attached to the left walls. These results strongly indicated that the standing microplates nucleated on the vertical walls when the receding contact line moved over the raised stripes, and then the nuclei grew into standing supercrystalline microplates along the direction perpendicular to the walls (Fig. 6d).

Accordingly, a possible mechanism for the formation of the parallel supercrystalline microplates standing on the trenches was proposed (Fig. 7). The receding of the contact line would bring about the nucleation of supercrystals with a smectic structure preferentially near the top edge of the trench wall with GNRs lying on the wall, which was followed by the addition of individual GNRs and their clusters to the nuclei in a side-by-side mode. As a result, the preferential growth along the directions perpendicular to parallel GNRs led to the formation of vertically aligned, supercrystalline microplates perpendicular to the parallel stripes. With the continuous movement of the contact line across the parallel stripes, a series of nearly parallel arrays of vertically aligned, supercrystalline microplates were obtained. However, it should be pointed out that this is just a very simplified model. As mentioned previously, the actual assembly processes may be much more complicated because of the unexpected perturbation during the assembly processes and the influence of the preformed microplates on the subsequent assembly of the neighboring microplates. It is noticeable that the microplates were not always attached to the right side of the

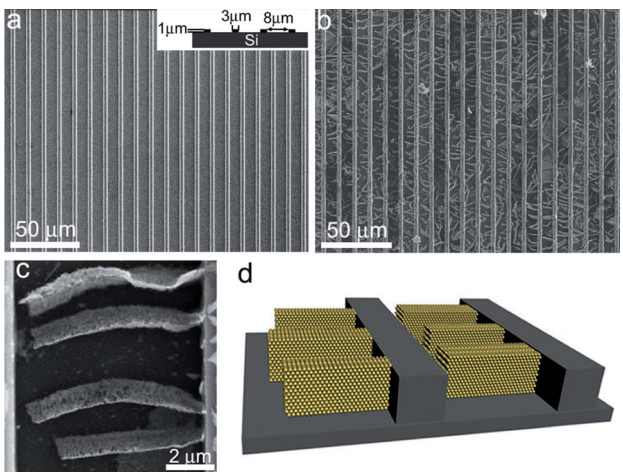

Fig. 6 (a) SEM image of the patterned substrate with parallely raised stripes. The inset schematically shows the side view of the substrate with the structural parameters labelled. (b and c) SEM images of the nearly parallel supercrystalline microplates assembled from GNRs. (d) Schematic illustration of parallel supercrystalline microplates standing on the trenches.

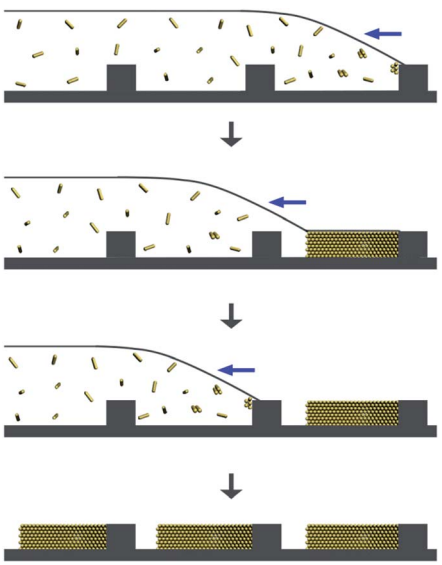

Fig. 7 Schematic illustration of the formation of vertically aligned, supercrystalline microplates perpendicular to the parallel stripes, showing the nucleation on the right walls of the trenches and the subsequent growth accompanying the gradual movement of the contact line. Blue arrows refer to the direction of contact line movement.

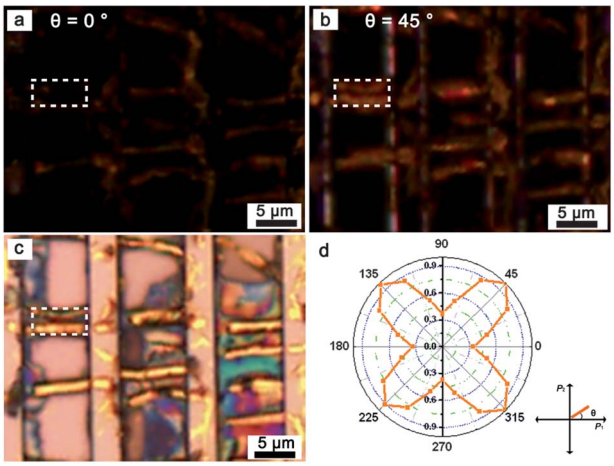

Fig. 8 (a and b) Cross-polarized micrographs of vertical supercrystalline microplates assembled from GNRs in the trenches on the stripe-patterned substrate with different angles between the length direction of the microplates and the polarizer direction (θ): (a) 0° and (b) 45°. (c) Optical micrograph of the vertical supercrystalline microplates. The colors from the area beside the microplates standing in the trenches arise from the interference of the CTAB film. (d) Polar plot of the integrated cross-polarized image brightness of a pair of nearly parallel microplates in the framed area as a function of the rotary angle θ.

trenches (Fig. 6b). This result might be ascribed to the abnormal nucleation at the middle of the trenches or at the left side of the trenches owing to the occasional perturbation of the meniscus and the contact line. It is expected that further optimization of the self-assembly process would lead to GNR supercrystal arrays with more accurate control over the uniformity and arrangement of supercrystalline building blocks.

The optical anisotropy of the nearly parallel arrays of supercrystalline microplates standing on the stripe-patterned substrate was also investigated using a cross-polarized optical microscope. As shown in Fig. 8a, all the nearly parallel microplates showed weak reflectance when the length direction of the microplates was approximately along the polarizer direction ($\theta \sim 0°$). They turned to bright synchronously when the microplates on the substrate were rotated 45° with respect to the polarizer direction (Fig. 8b). Fig. 8c shows the corresponding normal optical micrograph, which confirms that all the parallel microplates with $\theta \sim 45°$ showed strong reflectance as shown in Fig. 8b. The polar plot of the integrated cross-polarized image brightness of a pair of nearly parallel microplates standing on the trenches as a function of the rotary angle was measured, which is shown in Fig. 8d. As expected, the maximum or minimum reflectance repeats every 90°, which is very similar to the polar plot of a single microplate standing on the flat substrate shown in Fig. 5g. This result indicates that parallel supercrystalline microplates assembled by GNRs may be potentially integrated as useful optical devices with remarkable optical anisotropy.

Conclusions

Vertically aligned, supercrystalline microplates with a well-defined rectangular shape were fabricated in a large area through self-assembly of gold nanorods by a novel bulk solution evaporation method. This evaporative self-assembly strategy involving continuous movement of the contact line can prevent the coffee-ring effect, thus allowing uniform deposition of discrete GNR superstructures over a large area and favoring the formation of GNR supercrystals with geometrically symmetric shapes. A mechanism based on the continuing nucleation and growth of smectic GNR superstructures accompanying the movement of the contact line has been put forward for the formation of the unique GNR supercrystal arrays. Based on this mechanism, a micropatterned substrate was designed to control the nucleation location and growth direction, leading to the spontaneous self-assembly of nearly parallel arrays of vertically aligned, supercrystalline microplates of GNRs. This result provided a preliminary demonstration of the potential applications of the bulk solution evaporation combined with a micropatterned substrate in the assembly of GNR supercrystal arrays with controlled location and orientation. The obtained rectangular-plate-shaped GNR supercrystals exhibit interesting anisotropic optical reflection properties, and may provide opportunities for exploitation of metamaterials based on plasmonic supercrystals with well-defined shapes. Additionally, the self-assembly strategy involving the controlled contact line movement and the micropatterned substrate may open new avenues towards fabrication of well-defined supercrystals of anisotropic nanocrystals and arrangement of supercrystals into integrated devices.

Acknowledgements

This work was supported by NSFC (Grant nos. 21173010, 21073005, and 51121091) and MOST (Grant no. 2013CB932601).

Notes and references

1 Z. Nie, A. Petukhova and E. Kumacheva, *Nat. Nanotechnol.*, 2010, **5**, 15.
2 D. V. Talapin, J.-S. Lee, M. V. Kovalenko and E. V. Shevchenko, *Chem. Rev.*, 2010, **110**, 389.
3 D. Vanmaekelbergh, *Nano Today*, 2011, **6**, 419.
4 Z. Lu and Y. Yin, *Chem. Soc. Rev.*, 2012, **41**, 6874.
5 L. Xu, W. Ma, L. Wang, C. Xu, H. Kuang and N. A. Kotov, *Chem. Soc. Rev.*, 2013, **42**, 3114.
6 T. Wang, D. LaMontagne, J. Lynch, J. Zhuang and Y. C. Cao, *Chem. Soc. Rev.*, 2013, **42**, 2804.
7 Z. Quan and J. Fang, *Nano Today*, 2010, **5**, 390.
8 T. Huang, Q. Zhao, J. Xiao and L. Qi, *ACS Nano*, 2010, **4**, 4707.
9 K. Miszta, J. de Graaf, G. Bertoni, D. Dorfs, R. Brescia, S. Marras, L. Ceseracciu, R. Cingolani, R. van Roij, M. Dijkstra and L. Manna, *Nat. Mater.*, 2011, **10**, 872.
10 D. LaMontagne, H. Wu, Z. Wang and Y. C. Cao, *Science*, 2012, **338**, 358.
11 J. Henzie, M. Grünwald, A. Widmer-Cooper, P. L. Geissler and P. Yang, *Nat. Mater.*, 2012, **11**, 131.
12 J. Gong, G. Li and Z. Tang, *Nano Today*, 2012, **7**, 564.
13 S. J. Tan, M. J. Campolongo, D. Luo and W. Cheng, *Nat. Nanotechnol.*, 2011, **6**, 268.

14 (*a*) Z. Zhu, H. Meng, W. Liu, X. Liu, J. Gong, X. Qiu, L. Jiang, D. Wang and Z. Tang, *Angew. Chem., Int. Ed.*, 2011, **50**, 1593; (*b*) C.-W. Liao, Y.-S. Lin, K. Chanda, Y.-F. Song and M. H. Huang, *J. Am. Chem. Soc.*, 2013, **135**, 2684.
15 R. A. Alvarez-Puebla, A. Agarwal, P. Manna, B. P. Khanal, P. Aldeanueva-Potel, E. Carbó-Argibay, N. Pazos-Pérez, L. Vigderman, E. R. Zubarev, N. A. Kotov and L. M. Liz-Marzán, *Proc. Natl. Acad. Sci. U. S. A.*, 2011, **108**, 8157.
16 (*a*) Q. Liu, Y. Cui, D. Gardner, X. Li, S. He and I. I. Smalyukh, *Nano Lett.*, 2010, **10**, 1347; (*b*) S. Umadevi, X. Feng and T. Hegmann, *Adv. Funct. Mater.*, 2013, **23**, 1393; (*c*) S. Vial, D. Nykypanchuk, K. G. Yager, A. V. Tkachenko and O. Gang, *ACS Nano*, 2013, **7**, 5437.
17 L. Vigderman, B. P. Khanal and E. R. Zubarev, *Adv. Mater.*, 2012, **24**, 4811.
18 H. Chen, L. Shao, Q. Lia and J. Wang, *Chem. Soc. Rev.*, 2013, **42**, 2679.
19 S. E. Lohse and C. J. Murphy, *Chem. Mater.*, 2013, **25**, 1250.
20 T. Ming, X. Kou, H. Chen, T. Wang, H.-L. Tam, K.-W. Cheah, J.-Y. Chen and J. Wang, *Angew. Chem., Int. Ed.*, 2008, **47**, 9685.
21 A. Guerrero-Martínez, J. Pérez-Juste, E. Carbó-Argibay, G. Tardajos and L. M. Liz-Marzán, *Angew. Chem., Int. Ed.*, 2009, **48**, 9484.
22 Y. Xie, S. Guo, Y. Ji, C. Guo, X. Liu, Z. Chen, X. Wu and Q. Liu, *Langmuir*, 2011, **27**, 11394.
23 Y. Xie, Y. Jia, Y. Liang, S. Guo, Y. Ji, X. Wu, Z. Chen and Q. Liu, *Chem. Commun.*, 2012, **48**, 2128.
24 A. Petukhova, J. Greener, K. Liu, D. Nykypanchuk, R. Nicolay, K. Matyjaszewski and E. Kumacheva, *Small*, 2012, **8**, 731.
25 K. C. Ng, I. B. Udagedara, I. D. Rukhlenko, Y. Chen, Y. Tang, M. Premaratne and W. Cheng, *ACS Nano*, 2012, **6**, 925.
26 X. Ye, L. Jin, H. Caglayan, J. Chen, G. Xing, C. Zheng, V. Doan-Nguyen, Y. Kang, N. Engheta, C. R. Kagan and C. B. Murray, *ACS Nano*, 2012, **6**, 2804.
27 C. Hamon, M. Postic, E. Mazari, T. Bizien, C. Dupuis, P. Even-Hernandez, A. Jimenez, L. Courbin, C. Gosse, F. Artzner and V. Marchi-Artzner, *ACS Nano*, 2012, **6**, 4137.
28 T. Thai, Y. Zheng, S. Hock Ng, S. Mudie, M. Altissimo and U. Bach, *Angew. Chem., Int. Ed.*, 2012, **51**, 8732.
29 W. Han and Z. Lin, *Angew. Chem., Int. Ed.*, 2012, **51**, 1534.
30 F. Holzner, C. Kuemin, P. Paul, J. L. Hedrick, H. Wolf, N. D. Spencer, U. Duerig and A. W. Knoll, *Nano Lett.*, 2011, **11**, 3957.
31 C. Kuemin, R. Stutz, N. D. Spencer and H. Wolf, *Langmuir*, 2011, **27**, 6305.
32 C. Kuemin, L. Nowack, L. Bozano, N. D. Spencer and H. Wolf, *Adv. Funct. Mater.*, 2012, **22**, 702.
33 C. J. Orendorff and C. J. Murphy, *J. Phys. Chem. B*, 2006, **110**, 3990.
34 B. Gong, D. H. Kim and G. N. Parsons, *Langmuir*, 2012, **28**, 11906.
35 N. Nishiyama, S. Tanaka, Y. Egashira, Y. Oku and K. Ueyama, *Chem. Mater.*, 2003, **15**, 1006.
36 K. L. Young, M. R. Jones, J. Zhang, R. J. Macfarlane, R. Esquivel-Sirvent, R. J. Nape, J. Wu, G. C. Schatz, B. Lee and C. A. Mirkin, *Proc. Natl. Acad. Sci. U. S. A.*, 2012, **109**, 2240.
37 K. Park, H. Koerner and R. A. Vaia, *Nano Lett.*, 2010, **10**, 1433.
38 B. Peng, G. Li, D. Li, S. Dodson, Q. Zhang, J. Zhang, Y. H. Lee, H. V. Demir, X. Y. Ling and Q. Xiong, *ACS Nano*, 2013, **7**, 5993.